

# Unprecedentedly large superconducting gap in $\text{HgBa}_2\text{Ca}_2\text{Cu}_3\text{O}_{8+\delta}$ with the highest $T_c$ at ambient pressure

Chuanhao Wen<sup>1,4</sup>, Zhiyong Hou<sup>1,4</sup>, Alireza Akbari<sup>2,4</sup>, Kailun Chen<sup>1,4</sup>, Wenshan Hong<sup>3,4</sup>, Huan Yang<sup>1✉</sup>, Ilya Eremin<sup>2✉</sup>, Yuan Li<sup>3</sup>, and Hai-Hu Wen<sup>1✉</sup>

<sup>1</sup>Center for Superconducting Physics and Materials, National Laboratory of Solid State Microstructures and Department of Physics, Collaborative Innovation Center for Advanced Microstructures, Nanjing University, Nanjing 210093, China

<sup>2</sup>Institut für Theoretische Physik III, Ruhr-Universität Bochum, D-44801 Bochum, Germany

<sup>3</sup>International Center for Quantum Materials, School of Physics, Peking University, Beijing 100871, China

<sup>4</sup>These authors contributed equally: Chuanhao Wen, Zhiyong Hou, Alireza Akbari, Kailun Chen, Wenshan Hong.

✉e-mail: huanyang@nju.edu.cn; Ilya.Eremin@ruhr-uni-bochum.de; hhwen@nju.edu.cn

## Abstract

In cuprate superconductors, the highest superconducting transition temperature  $T_c$  is possessed by the  $\text{HgBa}_2\text{Ca}_2\text{Cu}_3\text{O}_{8+\delta}$  (Hg-1223) system at ambient pressure<sup>1</sup>, but the reason remains elusive. Here we report the scanning tunneling microscope measurements on the Hg-1223 single crystals with  $T_c \approx 134$  K. The observed superconducting gaps determined from the tunneling spectra can be categorized into two groups: the smaller gap  $\Delta_1$  ranges from about 45 to 70 meV, while the larger gap  $\Delta_2$  from about 65 to 98 meV. The observed unprecedentedly large gap value gives a straightforward explanation to the highest  $T_c$  in the Hg-1223 system. The largest gap observed here is comparable to the magnetic superexchange energy and excludes any possibility of using phonon pictures to interpret the superconductivity. Interestingly, an extremely strong particle-hole asymmetry is observed in associating with a very robust coherence peak at the bias of the larger gap in the hole branch of the Bogoliubov dispersion. We propose that the observed asymmetry results from the interplay of a flat band (van Hove singularity) in the electronic

**spectrum and the large superconducting gap in the underdoped layer. This could be the main reason for the strong pairing, and significant enhancement of the density of states in the hole branch of the Bogoliubov band yielding strong phase coherence of Cooper pairs. A scenario based on a trilayer model with an interlayer coupling can give a reasonable explanation. Our results provide deep insight into understanding the mechanism of superconductivity in cuprate superconductors.**

## **Main Text**

Since the discovery of high-temperature superconductivity in the cuprates<sup>2</sup> in 1986, substantial advancements have been achieved in theoretical and experimental studies. However, the underlying mechanism of superconductivity at such high temperatures is still an enigma and continues to be an essential topic of discussion in condensed matter physics<sup>3</sup>. Experimentally, the magnetic superexchange interaction between nearest-neighbour Cu spins may play a major role in the electron pairing<sup>4-8</sup>. Meanwhile, the electron-phonon coupling plays also some important roles in high- $T_c$  cuprates<sup>9-14</sup>. Consequently, the determining factor for the pairing strength—whether induced by phonon-mediated interaction, magnetic superexchange, or other factors, remains a challenging subject with ongoing debate. The comparison between the superconducting gaps and the characteristic energies of electron-electron or electron-phonon interaction can help solve the mystery of high- $T_c$  superconductivity in cuprates. To our knowledge, signatures of electron-phonon coupling were also reported in cuprate superconductors with the maximal phonon energies in different systems ranging from 50 to 80 meV, usually attributed to the optical branch of the phonon spectrum<sup>9-13</sup>, while the superexchange energy  $J$  is about 100~180 meV<sup>4-8,15</sup>. The central value of the larger superconducting gap previously observed in  $\text{Bi}_2\text{Sr}_2\text{Ca}_2\text{Cu}_3\text{O}_{10+\delta}$  is about 72 meV with the largest one exceeding 80 meV (Bi-2223)<sup>16</sup>. Thus, it is crucial to find whether the superconducting gap can have an energy scale significantly greater than the largest phonon energy, manifesting that there is limited space for using the electron-phonon coupling picture to interpret the superconducting mechanism in cuprates.

Among all superconductors, the  $\text{HgBa}_2\text{Ca}_2\text{Cu}_3\text{O}_{8+\delta}$  (Hg-1223) compound exhibits the highest critical temperature  $T_c \approx 134$  K at ambient pressure<sup>1</sup> ( $T_c$  reaches 164 K under pressure<sup>17</sup>). Like other trilayer cuprates<sup>18</sup>, Hg-1223 has three inequivalent  $\text{CuO}_2$  planes, i.e., one inner plane (IP) and two

outer planes (OPs) (Fig. 1a). Previous experiments have revealed that in the trilayer Bi-2223 system, the IP may be slightly underdoped while the OPs are overdoped<sup>19,20</sup>. Considering the positive correlation between the superconducting gap and the transition temperature, Hg-1223 is also expected to have a larger gap in the IP. This conclusion is strengthened by the reported gap enhancement induced by the Bogoliubov band hybridization in other trilayer cuprates<sup>21-23</sup>. However, due to the difficulty in preparing high-quality single crystals and the fact that this sample is not easy to cleave, there has been no report of studies on Hg-1223 using surface-sensitive probes, including scanning tunneling microscopy/spectroscopy (STM/STS) and angle-resolved photoemission spectroscopy (ARPES). Thus, the gap size and the reason for its highest  $T_c$  remain to be investigated in Hg-1223. In this article, STS measurements are conducted on optimally doped Hg-1223 samples. We observe two groups of superconducting gaps, presumably from the two bands of the IP and OPs, respectively. The largest gap can even reach a value of about 98 meV, significantly surpassing the scale of the available phonon frequencies. In addition, the intensity of the coherence peaks exhibits strong particle-hole asymmetry, and the intensity of the asymmetry has a roughly linear correlation with the larger gap size. We analyze our experimental results using trilayer model calculations and show that the particle-hole asymmetry of the coherence peaks for the larger gap could be a result of interesting interplay of the superconducting gap energy in the IP with the flat band (van Hove singularity). Such effect might enhance the Cooper pairs' phase coherence leading to additional boost for the superconducting transition temperature in Hg-1223 samples compared to other trilayer cuprates. Therefore, our findings contribute to a deeper understanding of the superconductivity mechanism in cuprate superconductors.

## Sample characterization

A typical topographic image measured on the cleaved surface of a Hg-1223 single crystal is shown in Fig. 1b. One can see that relatively flat surfaces can be observed on both sides of a distinct step edge. The height profile, along the path indicated by the orange arrow, reveals a height drop of 15.9 Å (Fig. 1c). This value is well consistent with the  $c$ -axis lattice parameter<sup>24</sup>  $c = 15.85$  Å. Unfortunately, we failed to obtain an atomic-resolved image. Unlike in Bi-family cuprates with two Bi-O planes connected by a van der Waals bond, the Hg-1223 has only one Hg-O plane in one unit cell, which prevents achieving an atomically resolved topography. As a result, after cleavage, the exposed surface is probably reconstructed by the residual Hg and O atoms without an apparent long-range atomic order.

Some clusters can be detected on the surface, which may be formed by Hg atoms. However, tunneling spectra with high quality can still be widely measured even with the tip traveling in a large distance on the surface.

Figure 1d shows the temperature-dependent in-plane resistivity of the Hg-1223 crystal, and the onset transition temperature  $T_c^{\text{onset}}$  is about 134 K. Figure 1e presents the temperature-dependent magnetic susceptibility measured at 10 Oe in zero-field-cooled and field-cooled modes. Both measurements show sharp superconducting transitions, indicative of high quality of the samples.

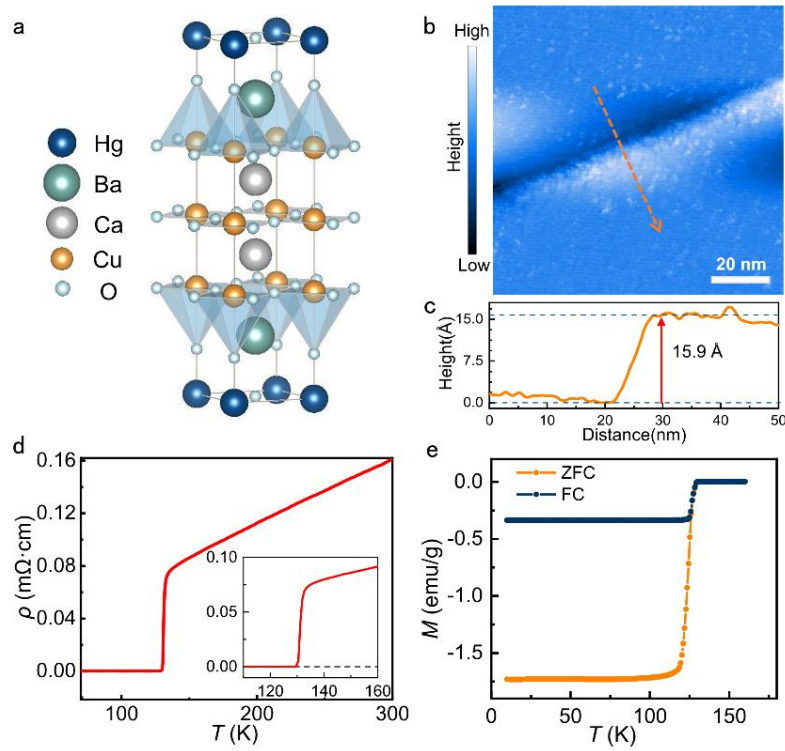


**Fig. 1: Crystal structure and sample characterization of Hg-1223.** **a**, Crystal structure of Hg-1223 in which two outer planes (OPs) and one inner plane (IP) are contained in a unit cell. **b**, Topography of the cleaved surface showing a single-unit-cell step. Setpoint condition:  $V_{\text{set}} = 1$  V,  $I_{\text{set}} = 20$  pA. **c**, Height profile obtained along the orange arrow shown in **b**. **d**, Temperature dependence of in-plane resistivity measured at 0 T. **e**, Temperature dependent magnetization measured in zero-field-cooled (ZFC) and field-cooled (FC) processes under a magnetic field of 10 Oe.

## Unprecedentedly large gap

Then, we conduct STS measurements on the cleaved surface to study the local density of states (LDOS). In Fig. 2b, we present three representative tunneling spectra measured in the area shown in Fig. 2a. Being consistent with other cuprate superconductors<sup>16,25-31</sup>, the spectra show the V-shaped feature near

zero bias, which is a characteristic feature of the  $d$ -wave pairing gap with the function of  $\Delta = \Delta_0 \cos(2\theta)$ , here  $\Delta_0$  is the gap maximum and  $\theta$  indicates the direction in momentum space relative to the "nodal" directions, which are along the diagonals of the Cu-O plaquettes. The presence of non-zero differential conductance at zero bias may be due to the impurity-scattering effect in a superconductor with a nodal sign-changing gap<sup>26,32</sup>. After a close inspection, these  $dI/dV$  curves show a two-gap feature, as marked by the arrows in Fig. 2b. Here we define the maximum of the smaller gap as  $\Delta_1$ , and the larger gap as  $\Delta_2$ . It is important to emphasize that the gap maximum approximates the energy of the coherence peak (kink) in a  $d$ -wave superconductor, especially when the scattering rate is low. Therefore, the larger gap  $\Delta_2$  is characterized by the coherence peak at a higher bias energy on the spectrum. In contrast, the smaller gap  $\Delta_1$  shows up as kinks. Strikingly, the coherence peak corresponding to the value of  $\Delta_2$  on the positive bias exhibits a very robust intensity.

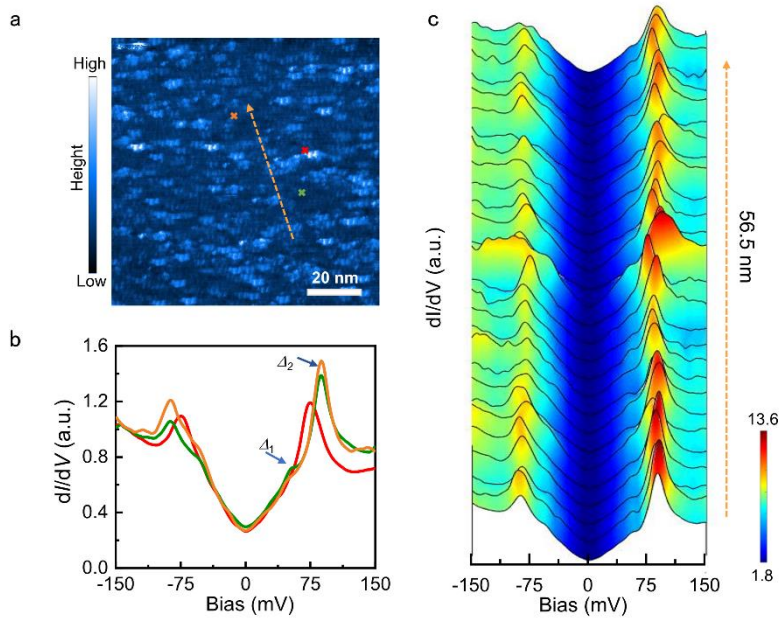


**Fig. 2: Spatially distribution of spectra and large gap.** **a**, STM topography of the cleaved surface. The clusters on the surface could potentially be scattered Hg/Ba atoms. **b**, Three tunneling spectra taken at the spots indicated by crosses with the corresponding colour in **a**. **c**, Spatially resolved tunneling spectra measured along the yellow dashed line in **a**. Each spectrum shows a two-gap feature, with the larger gap around 87meV. Setpoint condition: **a**,  $V_{\text{set}} = 1$  V,  $I_{\text{set}} = 20$  pA; **b,c**,  $V_{\text{set}} = 150$  mV,  $I_{\text{set}} = 200$  pA.

A sequence of tunneling spectra measured along the arrowed line in Fig. 2a is plotted in Fig. 2c. The two-gap feature can be seen on the spectra with the averaged gap maxima of  $\bar{\Delta}_1 \approx 57$  meV and

$\bar{\Delta}_2 \approx 87$  meV. Furthermore, both the peaks and the kinks are symmetric concerning the Fermi energy. We then use the Dynes model<sup>33</sup> with two  $d$ -wave gaps to fit the tunneling spectrum (Extended Data Fig. 1). The fitting curve captures the major characteristics on the negative-bias side but deviates strongly in the positive energy region, which will be discussed later. To our knowledge, the huge gap maximum  $\Delta_2 \approx 98$  meV observed in this study is the largest one ever reported, with the ratio  $2\Delta_2/k_B T_c \approx 17$  which far exceeds the expected value for the BCS theory in the weak coupling limit.

### Two groups of gap values

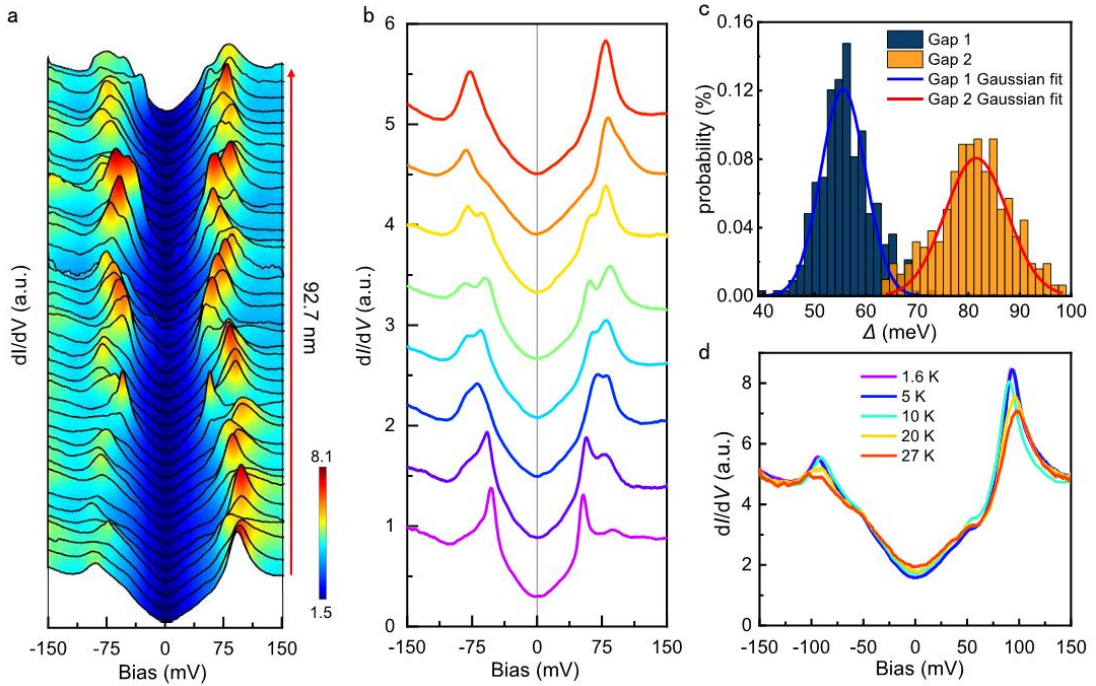


**Fig. 3: Energy distribution of the two superconducting gaps.** **a**, A set of tunneling spectra measured along the red line in Extended Data Fig. 2, which shows the ubiquitous inhomogeneity. **b**, Typical  $dI/dV$  curves with different contributions of the two gaps. **c**, Histogram of the superconducting gaps. The energy distribution of the probability is fitted by two Gaussian functions (the solid lines), and the peaks of the fitting curves locate at 56 meV and 82 meV, respectively. **d**, Tunneling spectra measured at the same position and at different temperatures. The coherence peaks at  $\Delta_2 \approx 93$  meV can be easily suppressed by increasing temperature. Setpoint condition:  $V_{\text{set}} = 150$  mV,  $I_{\text{set}} = 200$  pA.

In most places, the superconducting gaps show some inhomogeneous distribution, and an example is shown in Fig. 3a. It is evident that energies of the coherence peaks ( $\Delta_2$ ) or kinks ( $\Delta_1$ ) fluctuate dramatically, similar to the case in  $\text{Bi}_2\text{Sr}_2\text{CaCu}_2\text{O}_{8+\delta}$  (Bi-2212) and Bi-2223<sup>16,26,28,34</sup>. In addition, we

observe that the spectrum weights of the two gaps vary in different spectra. Some selective  $dI/dV$  curves with two-gap features are plotted in Fig. 3b. From the bottom curve up to the top one, there is a progressive increase in the spectrum-weight proportion of  $\Delta_2$ , while conversely, the proportion of  $\Delta_1$  exhibits a decreasing trend. Between the two extreme cases, spectra show two coherence peaks, which suggests a variable of contributed spectrum weight from the two gaps. The two-gap feature has also been observed on the spectra measured in another trilayer cuprate superconductor Bi-2223<sup>16,35</sup>.

Figure 3c presents a histogram showing the distribution of  $\Delta_2$  and  $\Delta_1$  obtained from the total of about 500  $dI/dV$  spectra measured in Hg-1223 samples. The distributions of the gap maxima behave as Gaussian functions for both gaps. Based on the fitting results, the peak energies are 56 and 82 meV for  $\Delta_1$  and  $\Delta_2$ , respectively. According to a commonly perceived result<sup>19,20</sup>, the IP and OPs are proved to be underdoped and overdoped, respectively. Therefore, it is reasonable to attribute the two superconducting gaps to these two different planes in Hg-1223. Since the coherence peaks are rather sharp, especially for the larger gap (see the top spectrum in Fig.3c), we do not think this large gap is a pseudogap, but instead it should have a superconducting origin.

In order to further rule out the possibility of a pseudogap, we examine the temperature-dependent and magnetic field evolution of the tunneling spectra. Figure 3d shows the  $dI/dV$  curves of the same position measured at different temperatures, on these curves the spectrum weight of the larger gap emerges as the predominant component. With the increase of temperature, the height of the coherence peaks corresponding to  $\Delta_2$  is steadily suppressed, and the zero-bias differential conductance rises concurrently. When comparing the spectra at 1.6 K and 27 K, it is observed that the height of the coherence peaks at  $E = +\Delta_2$  has reduced by approximately 15%. Furthermore, the tunneling spectra obtained under high magnetic fields (Extended Data Fig. 3) also show an effective suppression of the intensity of the coherence peaks at  $\pm\Delta_2$ . Based on these results, we can safely conclude that the coherence peaks at  $\pm\Delta_2$  must have a superconducting origin, instead of the pseudogap.

### **Strong particle-hole asymmetry**

As previously mentioned, the Dynes model fitting curve shows a deviation in the positive energy region, particularly around the coherence peak, see Extended Data Fig. 1. This deviation can be attributed to the fact that the larger gap has a stronger coherence peak at the positive bias. From our experiments, the coherence peak intensity at the positive energy side ( $P_+$ ) is clearly higher than that at

negative side ( $P_-$ ), but the energy values of the coherence peaks are symmetric about the Fermi level. Asymmetric tunneling spectra have been previously observed in cuprate superconductors<sup>36,37</sup>, but most of the asymmetry behaves as a higher coherence-peak intensity at negative energies than the positive energies<sup>26,28</sup>. Here in Hg-1223, the opposite situation occurs. To illustrate this asymmetry, we present one spectrum with the largest gap in Fig. 4a, and  $\Delta_2$  is as large as 98 meV. A remarkably strong and robust coherence peak is evident in the hole branch of the Bogoliubov dispersion. In contrast, the  $P_-$  is notably lower in comparison. Moreover, the spectrum measured on a broader energy window (Extended Data Fig. 4) shows that the background DOS at negative bias is even larger than that of positive energy, which confirms that the observed particle-hole asymmetry is not a result of the background density of states but rather an intrinsic characteristic of the superconducting state.

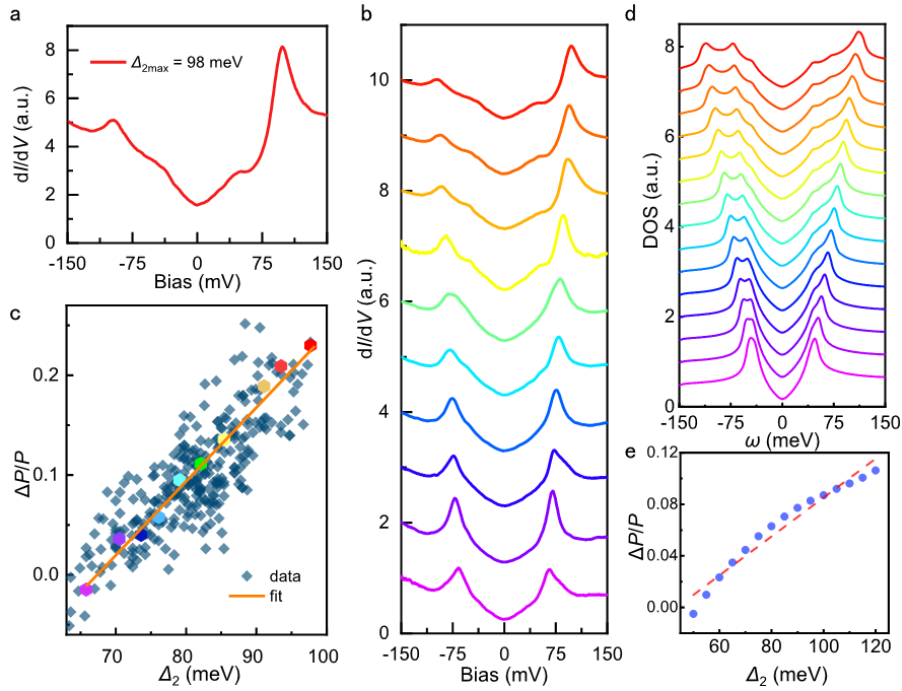


**Fig. 4: Particle-hole asymmetry in the coherence-peak height.** **a**, A tunneling spectrum with the largest  $\Delta_2$  of about 98 meV. The coherence peak at the positive bias is strong and robust. **b**, Tunneling spectra showing obvious particle-hole asymmetry. As the gap value increases, the positive coherence peak strengthens while the negative one gets suppressed. **c**, The intensity of the asymmetry  $\Delta P/P$  versus  $\Delta_2$ . The coloured hexagons come from the same-colored spectra that are displayed in **b**. The solid line represents the linear fitting result. Setpoint condition:  $V_{\text{set}} = 150$  mV,  $I_{\text{set}} = 200$  pA. **d**, Calculated DOS spectra for the trilayer model for various values of the larger superconducting gap  $\Delta_2$  (from 50 to 120 meV) by fixing  $\Delta_1 = 55$  meV,  $\Delta_{\text{OP}}^{(0)} \approx \Delta_1$  and  $\Delta_{\text{IP}}^{(0)} \approx \Delta_2$ . **e**, The resulting particle-hole asymmetry of the coherence peak at  $\Delta_2$ . Here the blue dots are the calculated values and the red dashed line is a guide to the eye.



Next, we focus on the impact of gap size on particle-hole asymmetry. Figure 4b shows a collection of some selected and normalized spectra, each corresponding to a different  $\Delta_2$  value ranging from 65 to 98 meV. A clear trend emerges as the gap size  $\Delta_2$  increases:  $P_+$  gets stronger, while  $P_-$  experiences a gradual suppression. To provide a quantitative description of this observed trend, we define a physical parameter,  $\Delta P/P = (P_+ - P_-)/(P_+ + P_-)$ , to represent the normalized difference between the intensities of coherence peaks at positive and negative biases. Figure 4c summarizes the asymmetry parameter  $\Delta P/P$  of the larger gap as a function of  $\Delta_2$ , and the data are shown as coloured hexagons. More data have been extracted from spectra with different gap sizes, and they are presented as blue squares in Fig. 4c. Interestingly,  $\Delta P/P$  demonstrates a positive and almost linear correlation with  $\Delta_2$ . As  $\Delta_2$  increases, the particle-hole asymmetry of coherence peaks becomes more pronounced. When the same statistical analysis is applied to  $\Delta_1$  (Extended Data Fig. 5), it is found that most values of  $\Delta P/P$  are negative, consistent with the background energy-dependent DOS (Extended Data Fig. 4). Moreover,  $\Delta P/P$  for  $\Delta_1$  shows a weaker and random distribution, and seems to be independent of  $\Delta_1$ .

## Model calculation

To model the three-CuO<sub>2</sub>-layer system we employ a tight-binding model for coupled CuO<sub>2</sub> planes, which has been previously used for Bi-2223 systems<sup>23</sup> and its details is presented in the Methods section. We note here that due to the absence of high-quality ARPES data at present in this compound one could use various set of the tight-binding parametrizations to find the reasonable fit to the experimental data. In particular, here we assume that the OP and IP bands are coupled primarily through the single-particle hopping between the OP and IP  $t_{\perp}(\mathbf{k}) = t_{\perp}^{(0)} + t_{\perp}^{(1)}(\cos k_x - \cos k_y)^2$  where  $t_{\perp}^{(0)} = 0$  and  $t_{\perp}^{(1)} = 15$  meV, which is similar to the values found for Bi-2223 compound<sup>42</sup>. We further assume that the intralayer electronic dispersions within each layer has the form  $\varepsilon_{i\mathbf{k}} = \frac{t_i}{2}(\cos k_x + \cos k_y) + t'_i \cos k_x \cos k_y + \frac{t''_i}{2}(\cos 2k_x + \cos 2k_y) + \mu_i$  where  $(t_i, t'_i, t''_i, \mu_i)$  refer to the intralayer hopping integrals between nearest, next-nearest, and next-next-nearest neighbors, respectively, as well as the chemical potential  $\mu_i$ . We choose the hopping integrals  $(t_{OP}, t'_{OP}, t''_{OP}, \mu_{OP}) = (-738, 120, -175, -24)$  meV for the outer (overdoped) planes and  $(t_{IP}, t'_{IP}, t''_{IP}, \mu_{IP}) = (-200, 33, -45, 62)$  meV for the inner (underdoped) plane. Most importantly,

the parametrization is chosen such that the flat band for the underdoped layer at  $\mu_i^{VHS} = -t'_i + t''_i + \mu_i$  is located at small negative bias, i.e., van Hove singularities (VHS) are located within the energy window of  $[-\Delta_i, \Delta_i]$  with respect to the Fermi level in the normal state as shown in Extended Data Fig. 6a. The superconducting gaps for the IP and OPs have a  $d$ -wave form  $\Delta_{i\mathbf{k}} = \frac{\Delta_i^{(0)}}{2}(\cos k_x - \cos k_y)$ . From previous data on Bi-2223 it is known that the interlayer Cooper-pairing tunneling gap  $\Delta_{\mathbf{k}}^{\text{inter}}$  is also of  $d$ -wave structure, dictated by symmetry but its magnitude is at most 10% of the intralayer gaps<sup>23</sup> and we checked that its inclusion does not change the results in a significant manner. The resulting Bogoliubov energy dispersion are shown in Extended Data Fig. 6b. The Green's function matrix for a superconducting state is defined as  $G(\mathbf{k}, i\omega) = [i\omega - \hat{H}_{\text{SC}}]^{-1}$  and the generalized density of states (DOS) is calculated in the continuum limit  $\rho(\omega) = -\frac{1}{\pi} \text{Im}[\sum_{\mathbf{k}} \text{Tr}'[G(\mathbf{k}, i\omega)]]_{i\omega \rightarrow \omega + i0^+}$ . To understand better the interplay between the superconducting gap magnitudes of OPs and IP and van Hove singularities we plot in Extended Data Fig. 7 the evolution of the DOS for varied magnitudes of the  $\Delta_{\text{OP}}^{(0)}$  and the  $\Delta_{\text{IP}}^{(0)}$  assuming for a fixed gap  $\Delta_1 = 55$  meV (inferred from the central value of experimental data, Fig. 3c), and  $\Delta_2$  is varied from 50 to 120 meV. As we show in the Methods for the single-band case the density of states of the Bogoliubov quasiparticles will show two features: the particle-hole symmetric coherence peaks at  $\omega \approx \pm \Delta_i$  and the particle-hole *asymmetric coherence-like* peaks at  $\omega \approx \pm \sqrt{(\mu_i^{VHS})^2 + \Delta_i^2}$  and the ratio of the asymmetry is determined whether  $\mu_i^{VHS}$  in the normal state is initially located at the positive or negative bias. For the negative bias, i.e.  $\mu_i^{VHS} < 0$ , the coherence-like peak is larger at positive bias and visa versa. In the situation when  $|\mu_i^{VHS}| \ll \Delta_i$  the two features merge into a single particle-hole asymmetric coherence-like peaks and the asymmetry is increasing the larger  $\Delta_i$  becomes. Note further that the single-band results would not explain the evolution of the experimental data and require an inclusion of the entire three-bands structure. For a chosen tight-binding parametrization in the three-bands case, the position of the van Hove singularity in the inner (underdoped) layer is located at the small negative energy in the normal state at around  $\mu_2^{VHS} \approx -16$  meV  $\ll \Delta_2$  and the resulting density of state shows a strong particle-hole asymmetry at  $\omega \approx \pm \sqrt{(\mu_2^{VHS})^2 + \Delta_2^2}$ , which is slightly larger than  $\omega \approx \Delta_2$ . The evolution of the density of states with various values of  $\Delta_2$  is further shown in Extended Data Fig. 7. Most importantly, we find that

the density of states shows three well-distinguishable features: two coherence peaks at  $\omega_1 \approx \pm \Delta_1$  and  $\omega_2 \approx \pm \Delta_2$  as well as particle-hole asymmetric coherence-like peaks at  $\omega_3 \approx \pm \sqrt{(\mu_2^{\text{VHS}})^2 + \Delta_2^2}$ . Note that the exact values depend on the shape of the Fermi surface for a fixed value of  $\Delta_i$  and the strength of the hybridization between different layers. The larger magnitude of  $\Delta_2$  is, the stronger is the particle-hole asymmetry of the peaks at  $\omega_3$  in qualitative agreement with the experimental data. To make a direct comparison to the experimental result we present the simulated data in the similar fashion as it is done in the experiment, see Fig. 4d in the main text. We further notice here that for detailed quantitative comparison further information on the electronic structure from the experiment would be needed, which is not available at present. At the same time, we believe that the presence of the flat band near the Fermi level in the trilayer Hg-1223 could be of significance to understand the origin of the highest  $T_c$  in this compound and deserves further investigation.

## Discussion

One of the most important issues is to find out what determines the critical temperature of a cuprate superconductor. Here, the most puzzling point is what characteristic enables Hg-1223 to host the highest critical temperature. Within cuprates, it is widely recognized that  $T_c$  is influenced by the number of  $\text{CuO}_2$  planes ( $n$ ) per unit cell, and it peaks at  $n = 3$  and begins to decline with a further increase of the number<sup>38</sup>  $n$ . In Bi-2223, enhanced gaps induced by Bogoliubov band hybridization between IP and OPs are observed<sup>21-23</sup>, which may be the cause of the relatively high  $T_c$ . At the same time, the interlayer gaps were found relatively moderate i.e. of the order of 10% of the intralayer gaps<sup>21-23</sup>. Given that Hg-1223 is also a trilayer cuprate, this phenomenon is expected to occur as well. Moreover, the measured superexchange energy  $J$  of Hg-1212 is larger than that of Bi-2223<sup>8</sup>. Consequently, it is logical to anticipate that Hg-1223, with higher  $T_c$ , will possess a larger  $J$  and, furthermore, will have a larger gap size as evidenced by our observations. Concerning the origin of the larger gap  $\Delta_2$ , we have provided several pieces of evidence to support that it is of a superconducting origin, and not a pseudogap. The observed unprecedentedly large gap may explain the highest  $T_c$  in the Hg-1223 system. Furthermore, the energy scale of  $\Delta_2$  exceeds the largest value of the phonon frequencies ever reported in all cuprate superconductor<sup>9-13</sup>. This may exclude the possibility of interpreting the superconductivity based on a phonon mediated picture.

Another surprising aspect we observed in our study is the strong particle-hole asymmetry of coherence peaks associated with the larger gap  $\Delta_2$  from the IP layer, although particle-hole asymmetry of coherence peaks was also reported in Bi-2223 and was attributed to the pair-breaking scattering between flat antinodal Bogoliubov bands<sup>39</sup>. As follows from our analysis the particle-hole asymmetry of the coherence-like peaks in Hg-1223 may stem from the interplay of the VHS singularity from the normal state electronic spectrum with the superconducting gap energy in the IP layer, which points towards another possible mechanism of  $T_c$  enhancement in these trilayer systems. This is certainly beyond BCS paradigm and requires further analysis. Previous ARPES studies have revealed that the height of superconducting coherence peaks is proportional to the superfluid density<sup>40,42</sup>. This complicated electronic structure enables Hg-1223 to possess considerable pairing strength and strong phase stiffness at the same time, which may account for the highest<sup>43</sup>  $T_c$ . Given the new insight, a promising way to further enhance  $T_c$  could be to band-engineer the location of VHS relative to the Fermi level, so that its interplay with the superconducting gap can help boost the phase coherence of Cooper pairing.

## References

- 1 Schilling, A., Cantoni, M., Guo, J. D. & Ott, H. R. Superconductivity above 130 K in the Hg–Ba–Ca–Cu–O system. *Nature* **363**, 56–58 (1993).
- 2 Bednorz, J. G. & Müller, K. A. Possible high  $T_c$  superconductivity in the Ba-La-Cu-O system. *Z. Phys. B: Condens. Matter* **64**, 189–193 (1986).
- 3 Keimer, B., Kivelson, S. A., Norman, M. R., Uchida, S. & Zaanen, J. From quantum matter to high-temperature superconductivity in copper oxides. *Nature* **518**, 179–186 (2015).
- 4 Tokura, Y. *et al.* Cu-O network dependence of optical charge-transfer gaps and spin-pair excitations in single-CuO<sub>2</sub>-layer compounds. *Phys. Rev. B* **41**, 11657–11660 (1990).
- 5 Aronson, M. C., Dierker, S. B., Dennis, B. S., Cheong, S. W. & Fisk, Z. Pressure dependence of the superexchange interaction in antiferromagnetic La<sub>2</sub>CuO<sub>4</sub>. *Phys. Rev. B* **44**, 4657–4660 (1991).
- 6 Le Tacon, M. *et al.* Intense paramagnon excitations in a large family of high-temperature superconductors. *Nat. Phys.* **7**, 725–730 (2011).
- 7 O'Mahony, S. M. *et al.* On the electron pairing mechanism of copper-oxide high temperature superconductivity. *Proc. Natl Acad. Sci.* **119**, e2207449119 (2022).
- 8 Wang, L. *et al.* Paramagnons and high-temperature superconductivity in a model family of

- cuprates. *Nat. Commun.* **13**, 3163 (2022).
- 9 Lanzara, A. *et al.* Evidence for ubiquitous strong electron–phonon coupling in high-temperature superconductors. *Nature* **412**, 510–514 (2001).
- 10 Cuk, T. *et al.* A review of electron-phonon coupling seen in the high- $T_c$  superconductors by angle-resolved photoemission studies (ARPES). *Physica Status Solidi (b)* **242**, 11–29 (2005).
- 11 Lee, W. S. *et al.* Role of Lattice coupling in establishing electronic and magnetic properties in quasi-one-dimensional cuprates. *Phys. Rev. Lett.* **110**, 265502 (2013).
- 12 Wang, Y. *et al.* Phonon-mediated long-range attractive interaction in one-dimensional cuprates. *Phys. Rev. Lett.* **127**, 197003 (2021).
- 13 Chen, Z. *et al.* Anomalously strong near-neighbor attraction in doped 1D cuprate chains. *Science* **373**, 1235–1239 (2021).
- 14 He, Y. *et al.* Rapid change of superconductivity and electron-phonon coupling through critical doping in Bi-2212. *Science* **362**, 62–65 (2018).
- 15 Peng, Y. Y. *et al.* Influence of apical oxygen on the extent of in-plane exchange interaction in cuprate superconductors. *Nat. Phys.* **13**, 1201–1206 (2017).
- 16 Hao, Z. *et al.* Anomalous doping evolution of superconductivity and quasiparticle interference in  $\text{Bi}_2\text{Sr}_2\text{Ca}_2\text{Cu}_3\text{O}_{10+\delta}$  trilayer cuprates. *Phys. Rev. Lett.* **125**, 237005 (2020).
- 17 Gao, L. *et al.* Superconductivity up to 164 K in  $\text{HgBa}_2\text{Ca}_{m-1}\text{Cu}_m\text{O}_{2m+2+\delta}$  ( $m = 1, 2, \text{ and } 3$ ) under quasihydrostatic pressures. *Phys. Rev. B* **50**, 4260–4263 (1994).
- 18 Mukuda, H., Shimizu, S., Iyo, A. & Kitaoka, Y. High- $T_c$  superconductivity and antiferromagnetism in multilayered copper oxides – a new paradigm of superconducting mechanism. *J. Phys. Soc. Jpn.* **81**, 011008 (2011).
- 19 Kotegawa, H. *et al.* NMR study of carrier distribution and superconductivity in multilayered high- $T_c$  cuprates. *J. Phys. Chem. Solids* **62**, 171-175 (2001).
- 20 Ideta, S. *et al.* Enhanced superconducting gaps in the trilayer high-temperature  $\text{Bi}_2\text{Sr}_2\text{Ca}_2\text{Cu}_3\text{O}_{10+\delta}$  cuprate superconductor. *Phys. Rev. Lett.* **104**, 227001 (2010).
- 21 Kunisada, S. *et al.* Observation of bogoliubov band hybridization in the optimally doped trilayer  $\text{Bi}_2\text{Sr}_2\text{Ca}_2\text{Cu}_3\text{O}_{10+\delta}$ . *Phys. Rev. Lett.* **119**, 217001 (2017).
- 22 Ideta, S. *et al.* Hybridization of bogoliubov quasiparticles between adjacent  $\text{CuO}_2$  layers in the triple-layer cuprate  $\text{Bi}_2\text{Sr}_2\text{Ca}_2\text{Cu}_3\text{O}_{10+\delta}$  studied by angle-resolved photoemission spectroscopy. *Phys. Rev. Lett.* **127**, 217004 (2021).
- 23 Luo, X. *et al.* Electronic origin of high superconducting critical temperature in trilayer cuprates. *Nat. Phys.* **19**, 1841–1847 (2023).
- 24 Shao, H. M. *et al.* Synthesis and X-ray powder diffraction analysis of the high- $T_c$  superconductor  $\text{HgBa}_2\text{Ca}_2\text{Cu}_3\text{O}_{8+\delta}$ . *Solid State Commun* **92**, 595–599 (1994).
- 25 Renner, C. & Fischer, O. Vacuum tunneling spectroscopy and asymmetric density of states of  $\text{Bi}_2\text{Sr}_2\text{CaCu}_2\text{O}_{8+\delta}$ . *Phys. Rev. B* **51**, 9208–9218 (1995).

- 26 Pan, S. H. *et al.* Microscopic electronic inhomogeneity in the high- $T_c$  superconductor  $\text{Bi}_2\text{Sr}_2\text{CaCu}_2\text{O}_{8+x}$ . *Nature* **413**, 282–285 (2001).
- 27 Jenkins, N. *et al.* Imaging the essential role of spin fluctuations in high- $T_c$  superconductivity. *Phys. Rev. Lett.* **103**, 227001 (2009).
- 28 Gu, Q. *et al.* Directly visualizing the sign change of  $d$ -wave superconducting gap in  $\text{Bi}_2\text{Sr}_2\text{CaCu}_2\text{O}_{8+\delta}$  by phase-referenced quasiparticle interference. *Nat. Commun.* **10**, 1603 (2019).
- 29 Yuli, O. *et al.* Enhancement of the superconducting transition temperature of  $\text{La}_{2-x}\text{Sr}_x\text{CuO}_4$  bilayers: role of pairing and phase stiffness. *Phys. Rev. Lett.* **101**, 057005 (2008).
- 30 Hanaguri, T. *et al.* Quasiparticle interference and superconducting gap in  $\text{Ca}_{2-x}\text{Na}_x\text{CuO}_2\text{Cl}_2$ . *Nat. Phys.* **3**, 865–871 (2007).
- 31 He, Y. *et al.* Fermi surface and pseudogap evolution in a cuprate superconductor. *Science* **344**, 608–611 (2014).
- 32 McElroy, K. *et al.* Atomic-scale sources and mechanism of nanoscale electronic disorder in  $\text{Bi}_2\text{Sr}_2\text{CaCu}_2\text{O}_{8+\delta}$ . *Science* **309**, 1048–1052 (2005).
- 33 Dynes, R. C., Narayanamurti, V. & Garno, J. P. Direct measurement of quasiparticle-lifetime broadening in a strong-coupled superconductor. *Phys. Rev. Lett.* **41**, 1509–1512 (1978).
- 34 Kugler, M. *et al.* Scanning tunneling spectroscopy on  $\text{Bi}_2\text{Sr}_2\text{Ca}_2\text{Cu}_3\text{O}_{10+\delta}$  single crystals. *J. Phys. Chem. Solids* **67**, 353–356 (2006).
- 35 Zou, C. *et al.* Effect of structural supermodulation on superconductivity in trilayer cuprate  $\text{Bi}_2\text{Sr}_2\text{Ca}_2\text{Cu}_3\text{O}_{10+\delta}$ . *Phys. Rev. Lett.* **124**, 047003 (2020).
- 36 Anderson, P. W. & Ong, N. P. Theory of asymmetric tunneling in the cuprate superconductors. *J. Phys. Chem. Solids* **67**, 1–5 (2006).
- 37 Hirsch, J. E. Slope of the superconducting gap function in  $\text{Bi}_2\text{Sr}_2\text{CaCu}_2\text{O}_{8+\delta}$  measured by vacuum tunneling spectroscopy. *Phys. Rev. B* **59**, 11962–11973 (1999).
- 38 Chakravarty, S., Kee, H.-Y. & Völker, K. An explanation for a universality of transition temperatures in families of copper oxide superconductors. *Nature* **428**, 53–55 (2004).
- 39 Zou, C. *et al.* Particle-hole asymmetric superconducting coherence peaks in overdoped cuprates. *Nat. Phys.* **18**, 551–557 (2022).
- 40 Feng, D. L. *et al.* Signature of superfluid density in the single-particle excitation spectrum of  $\text{Bi}_2\text{Sr}_2\text{CaCu}_2\text{O}_{8+\delta}$ . *Science* **289**, 277–281 (2000).
- 41 Ding, H. *et al.* Coherent quasiparticle weight and its connection to high- $T_c$  superconductivity from angle-resolved photoemission. *Phys. Rev. Lett.* **87**, 227001 (2001).
- 42 Emery, V. J. & Kivelson, S. A. Importance of phase fluctuation in superconductors with small superfluid density. *Nature* **374**, 434–437(1995).
- 43 Anderson, O. K. *et al.* LDA energy bands, low-energy hamiltonians,  $t'$ ,  $t''$ ,  $t_\perp$  (k), and  $J_\perp$ ,  $J$ . *Phys. Chem. Solids* **56**, 1573–1591 (1995).

## Acknowledgements

We acknowledge helpful discussions with Tao Xiang at IOP, CAS and Qianghua Wang at NJU. This work was supported by the National Natural Science Foundation of China (Grant Nos. NSFC-DFG/12061131001, 11927809, 12061131004, 11888101) and National Key R&D Program of China (Grant No. 2022YFA1403201, 2021YFA1401900). The work of I. E. and A. A. is supported by the German Research Foundation within the bilateral NSFC-DFG Project No. ER 463/14-1. W. H. acknowledges support from the Postdoctoral Innovative Talent program (BX2021018) and the China Postdoctoral Science Foundation (2021M700250).

## Author contributions

Single crystals were synthesized by W.H. and Y.L. STM/STS measurements and analysis were performed by C.W., Z.H., K.C., H.Y. and H.H.W. The theoretical calculation was done by A.A. and I.E. H.H.W., H.Y., C.W., and I.E. wrote the paper. H.H.W. coordinated the whole work. All authors have discussed the results and the interpretations.

## Competing interests

The authors declare no competing interests.

## Methods

**Sample preparation and characterization.** Optimally doped  $\text{HgBa}_2\text{Ca}_2\text{Cu}_3\text{O}_{8+\delta}$  single crystals were grown with a self-flux method<sup>44</sup>. Temperature-dependent resistivity measurements were carried out with a physical property measurement system (PPMS-9T, Quantum Design). The DC magnetization measurements were performed with a SQUID-VSM-7T (Quantum Design).

**STM/STS measurements.** The STM/STS measurements were carried out in a scanning tunneling microscope (USM-1300, Unisoku Co., Ltd.) with ultra-high vacuum, low temperature, and high magnetic field. The samples were cleaved in an ultra-high vacuum with a base pressure of about  $1 \times 10^{-10}$  torr at liquid nitrogen temperatures. The electrochemically etched tungsten tips were used for the STM/STS measurements. A typical lock-in technique was used for the tunneling spectrum

measurements with an AC modulation of 3mV and 931.773 Hz. The offset bias voltages in STS measurements have been carefully calibrated. The STM/STS measurements are carried at 1.6 K except for the variable temperature measurements.

## Details of theoretical model

For a three-CuO<sub>2</sub>-layer system, the electronic band structure in the superconducting state can be described by the following generic 6×6 Hamiltonian matrix in the Nambu-Gor'kov basis, which was previously employed for the description of Bi-2223 trilayer cuprates<sup>22</sup>:

$$\hat{H}_{SC} = \Phi^\dagger \begin{pmatrix} \varepsilon_{OP}(\mathbf{k}) & t_{IO}(\mathbf{k}) & t_{OO}(\mathbf{k}) & \Delta_{OP}(\mathbf{k}) & \Delta_{IO}(\mathbf{k}) & \Delta_{OO}(\mathbf{k}) \\ t_{IO}(\mathbf{k}) & \varepsilon_{IP}(\mathbf{k}) & t_{IO}(\mathbf{k}) & \Delta_{IO}(\mathbf{k}) & \Delta_{IP}(\mathbf{k}) & \Delta_{IO}(\mathbf{k}) \\ t_{OO}(\mathbf{k}) & t_{IO}(\mathbf{k}) & \varepsilon_{OP}(\mathbf{k}) & \Delta_{OO}(\mathbf{k}) & \Delta_{IO}(\mathbf{k}) & \Delta_{OP}(\mathbf{k}) \\ \Delta_{OP}(\mathbf{k}) & \Delta_{IOP}(\mathbf{k}) & \Delta_{OO}(\mathbf{k}) & -\varepsilon_{OP}(\mathbf{k}) & -t_{IO}(\mathbf{k}) & -t_{OO}(\mathbf{k}) \\ \Delta_{IOP}(\mathbf{k}) & \Delta_{IP}(\mathbf{k}) & \Delta_{IOP}(\mathbf{k}) & -t_{IO}(\mathbf{k}) & -\varepsilon_{IP}(\mathbf{k}) & -t_{IO}(\mathbf{k}) \\ \Delta_{OO}(\mathbf{k}) & \Delta_{IOP}(\mathbf{k}) & \Delta_{OP}(\mathbf{k}) & -t_{OO}(\mathbf{k}) & -t_{IO}(\mathbf{k}) & -\varepsilon_{OP}(\mathbf{k}) \end{pmatrix} \Phi \quad (1)$$

Here the bare band dispersion of the inner plane,  $\varepsilon_{IP}(\mathbf{k})$ , and outer planes,  $\varepsilon_{OP}(\mathbf{k})$ , can be described by the tight-binding parametrization  $\varepsilon_i(\mathbf{k}) = \frac{1}{2}t_i(\cos k_x + \cos k_y) + t'_i \cos k_x \cos k_y + \frac{1}{2}t''_i(\cos 2k_x + \cos 2k_y) + \mu_i$  where  $t_i$ ,  $t'_i$ ,  $t''_i$  are the in-plane nearest-neighbor, second-nearest-neighbor and third-nearest-neighbor in-plane hoppings, respectively. The hybridization between the planes is given by  $t_i(\mathbf{k}) = t_i^{(0)} + t_i^{(1)}(\cos k_x - \cos k_y)^2$ . The *d*-wave superconducting gaps in the outer (overdoped) and inner (underdoped) planes are defined as  $\Delta_{OP}(\mathbf{k}) = \Delta_1(\mathbf{k}) = \frac{\Delta_1}{2}(\cos k_x - \cos k_y)$  and  $\Delta_{IP}(\mathbf{k}) = \Delta_2(\mathbf{k}) = \frac{\Delta_2}{2}(\cos k_x - \cos k_y)$  where index 1 and 2 refer to assignment of the gaps found in experiment. For the sake of simplicity, we assume that the interlayer gaps  $\Delta_{IO}(\mathbf{k})$  and  $\Delta_{OO}(\mathbf{k})$  are small and we checked that their inclusion do not alter our main conclusion. Similarly, we assumed that the hybridization occurs only between nearest CuO<sub>2</sub> planes and  $t_{OO}(\mathbf{k})$  can be also neglected. We note here that its inclusion would not change the major details of the interpretation but would certainly be needed once high-quality ARPES data become available.

We calculate the generalized Density of States (DOS) in the continuum limit as

$$\rho(\omega) = -\frac{1}{\pi} \text{Im}[\sum_{\mathbf{k}} \text{Tr}'(G(\mathbf{k}, i\omega))]_{i\omega \rightarrow \omega + i0^+} \quad (2)$$

where  $\text{Tr}'$  acts only on the particle part of the particle-hole Nambu-Gor'kov basis and



$$G(\mathbf{k}, i\omega) = [i\omega - \hat{H}_{SC}]^{-1} \quad (3)$$

is the Nambu-Gorkov Green's function in the superconducting state.

To understand the origin of the particle-hole asymmetry of the Bogoliubov coherence-like peaks let us start by considering a single-band describing a given layer without any hybridization to the adjacent layers. In such a case the expression for the density of states simplifies to

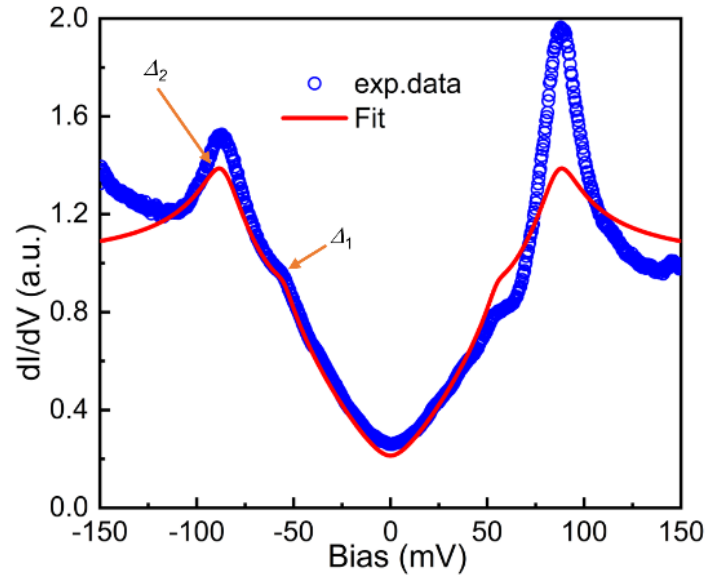
$$\rho_{sb}(\omega) = \int \frac{d^2\mathbf{k}}{4\pi^2} [u_{i\mathbf{k}}^2 \delta(\omega - E_i(\mathbf{k})) + v_{i\mathbf{k}}^2 \delta(\omega + E_i(\mathbf{k}))] \quad (4)$$

where  $E_i(\mathbf{k}) = \sqrt{\varepsilon_i^2(\mathbf{k}) + \Delta_i^2}$  is the superconducting energy dispersion and  $u_{i\mathbf{k}}^2 = \frac{1}{2} \left[ 1 + \frac{\varepsilon_i(\mathbf{k})}{E_i(\mathbf{k})} \right]$  and  $v_{i\mathbf{k}}^2 = \frac{1}{2} \left[ 1 - \frac{\varepsilon_i(\mathbf{k})}{E_i(\mathbf{k})} \right]$  are the Bogoliubov coefficients. In the situation when the normal state dispersion  $\varepsilon_i(\mathbf{k})$  possesses a flat band (Van Hove singularity at  $(\pm\pi, 0)$  and  $(0, \pm\pi)$ ) points of the Brollouin Zone) located at  $\mu_i^{VHS} = -t'_i + t''_i + \mu_i$ . The density of states will show two features: the particle-hole symmetric coherence peaks at  $\omega \approx \pm \Delta_i$  and the particle-hole *asymmetric coherence-like* peaks at  $\omega \approx \pm \sqrt{(\mu_i^{VHS})^2 + \Delta_i^2}$  and the ratio of the asymmetry is determined whether  $\mu_i^{VHS}$  in the normal state is initially located at the positive or negative bias. For the negative bias, i.e.  $\mu_i^{VHS} < 0$ , the coherence-like peak is larger at positive bias and visa versa. In the situation when  $|\mu_i^{VHS}| \ll \Delta_i$  the two features merge into a single particle-hole asymmetric coherence-like peaks and the asymmetry is increasing the larger  $\Delta_i$  becomes.

In Extended Data Fig. 6, we present the full energy dispersion of the three-band model in the normal state (a) and the quasiparticle spectral density in the superconducting state,  $A(\mathbf{k}, \omega) = -\frac{1}{\pi} \text{Im}[\text{Tr}'(G(\mathbf{k}, i\omega))]_{i\omega \rightarrow \omega + i0^+}$  (b) using exemplarily  $\Delta_1 = 55$  meV and  $\Delta_2 = 100$ meV along the high-symmetry route of the first Brollouine Zone. The evolution of the density of states with various values of  $\Delta_2$  is further shown in Extended Data Fig. 7.

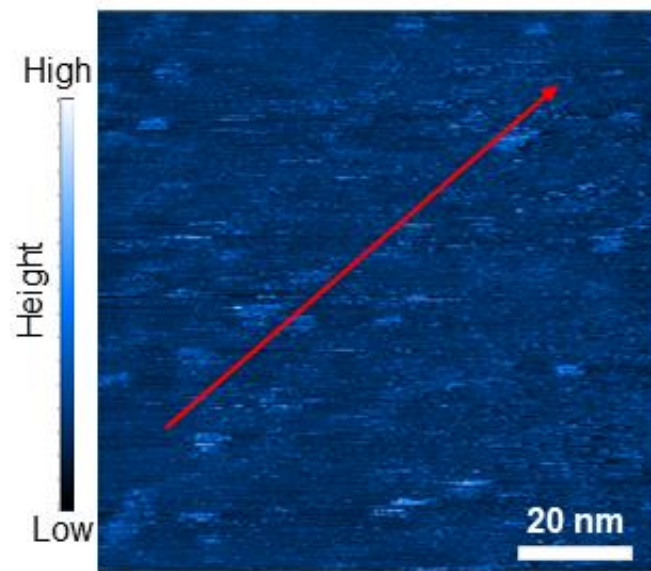
44 Wang, L. *et al.* Growth and characterization of HgBa<sub>2</sub>CaCu<sub>2</sub>O<sub>6+δ</sub> and HgBa<sub>2</sub>Ca<sub>2</sub>Cu<sub>3</sub>O<sub>8+δ</sub> crystals. *Phys. Rev. Mater.* **2**, 123401 (2018).

## Extended Data

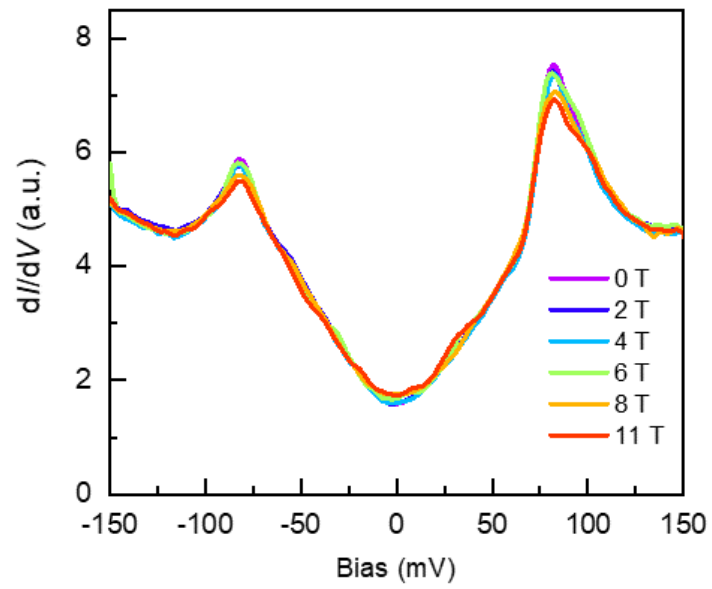


**Extended Data Fig. 1: Dynes model fitting to a tunneling spectrum with the two-gap feature.**

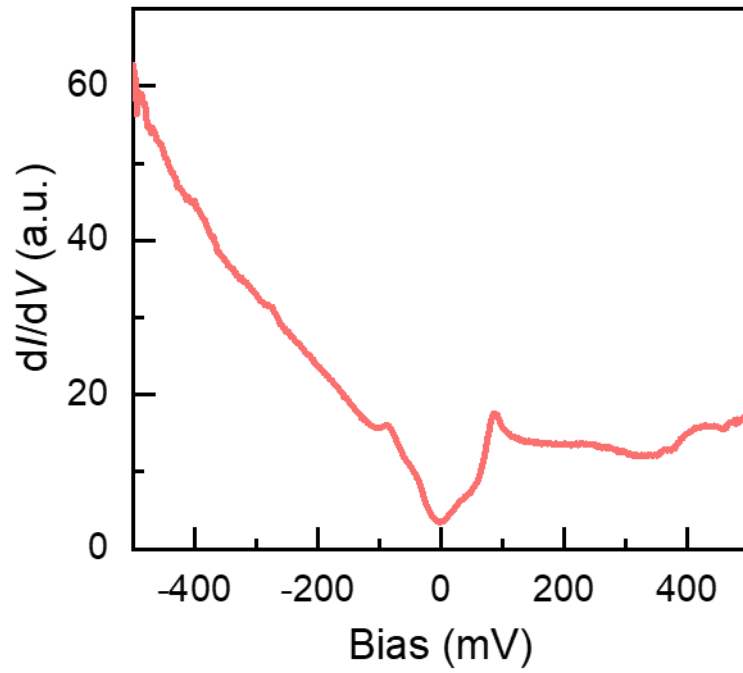
Fitting parameters:  $\Delta_1 = 55$  meV,  $\Gamma_1 = 12$  meV,  $\Delta_2 = 87$  meV,  $\Gamma_2 = 4$  meV. The arrows indicate the energies of the superconducting gap maxima obtained by the fitting. One can see that the energies of the coherence peak or the kink are close to the gap maxima.



**Extended Data Fig. 2: STM topography of an area.** The spatially resolved tunneling spectra in Fig. 3a are measured along the red line. Setpoint condition:  $V_{\text{set}} = 1 \text{ V}$ ,  $I_{\text{set}} = 20 \text{ pA}$ .

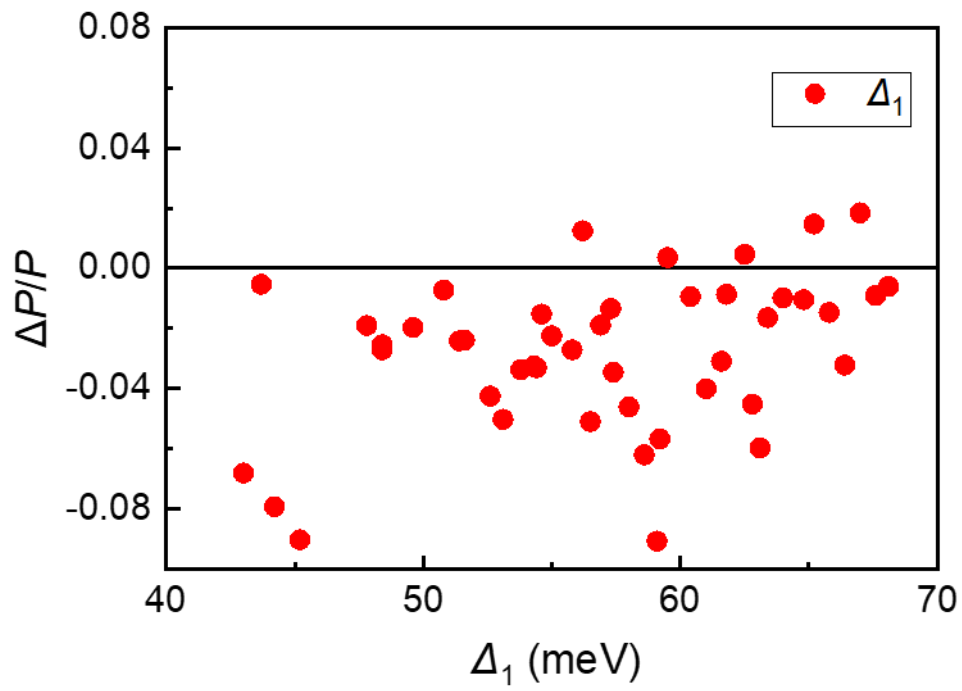


**Extended Data Fig. 3: Tunneling spectra measured at different magnetic fields.** The coherence peaks at  $\Delta_2 = 87$  meV can be suppressed by the magnetic field. Setpoint condition:  $V_{\text{set}} = 150$  mV,  $I_{\text{set}} = 200$  pA.

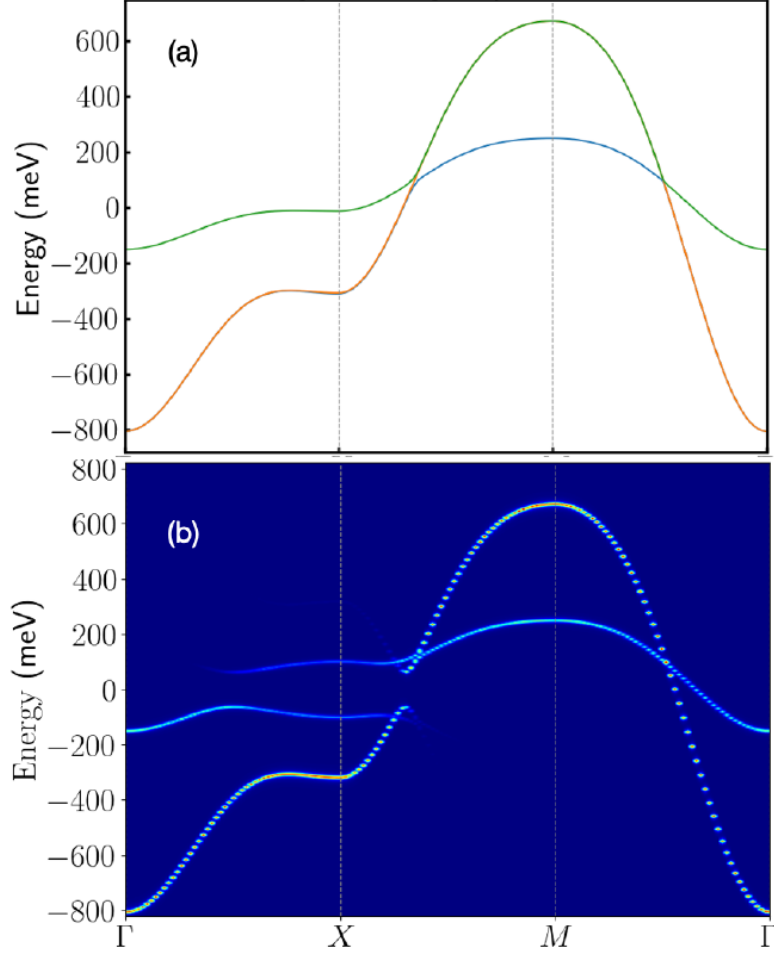


**Extended Data Fig. 4: Tunneling spectra measured in a wider range and statistical analysis of  $\Delta_1$ .**

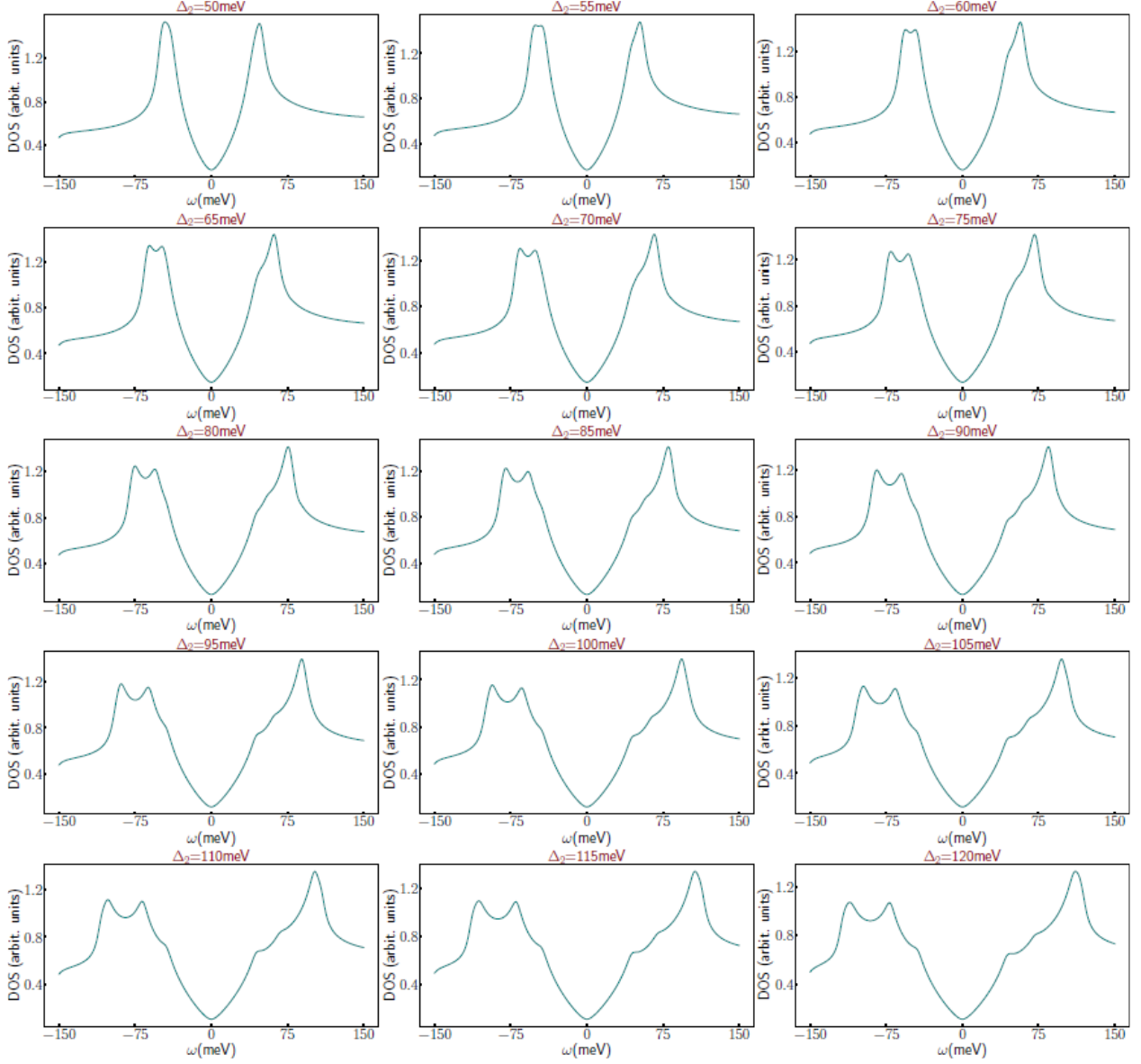
A typical tunneling spectrum measured in an energy window far beyond the superconducting gap. The background DOS at negative bias is even larger than that of positive energy. Setpoint condition:  $V_{\text{set}} = 500$  mV,  $I_{\text{set}} = 1$  nA.



**Extended Data Fig. 5: The intensity of the coherence-peak asymmetry  $\Delta P/P$  versus  $\Delta_1$ .** Since there is no clear relationship between  $\Delta P/P$  and  $\Delta_1$ , we show data of some spectra.



**Extended Data Fig. 6:** Trilayer electronic band structure in the normal (a) and superconducting (b) states using the following hopping parameters  $(t_{OP}, t'_{OP}, t''_{OP}, \mu_{OP}) = (-738, 120, -175, -24)$  meV and  $(t_{IP}, t'_{IP}, t''_{IP}, \mu_{IP}) = (-200, 33, -45, 62)$  meV assuming weak hybridization between the layers,  $t_{IO}^{(0)} = 0$  and  $t_{IO}^{(1)} = 15$  meV (b) shows the quasiparticle spectral density in the superconducting state,  $A(\mathbf{k}, \omega) = -\frac{1}{\pi} \text{Im}[\text{Tr}'(G(\mathbf{k}, i\omega))]_{i\omega \rightarrow \omega + i0^+}$  with  $\Delta_1 = 55$  meV and  $\Delta_2 = 100$  meV. Observe a near degeneracy of the onset of the Bogoliubov dispersion  $\omega \approx \pm \Delta_2$  and the position of the corresponding flat band at  $\omega \approx \pm \sqrt{(\mu_2^{\text{VHS}})^2 + \Delta_2^2}$ .



**Extended Data Fig.7:** Calculated evolution of the quasiparticle density of states for various values of  $\Delta_2$  with a fixed value of  $\Delta_1 = 55$  meV. The normal state parameters are described in the text and are the same as in Extended Data Fig.6.